

Journal of Materials Chemistry A

Accepted Manuscript



This is an *Accepted Manuscript*, which has been through the Royal Society of Chemistry peer review process and has been accepted for publication.

Accepted Manuscripts are published online shortly after acceptance, before technical editing, formatting and proof reading. Using this free service, authors can make their results available to the community, in citable form, before we publish the edited article. We will replace this *Accepted Manuscript* with the edited and formatted *Advance Article* as soon as it is available.

You can find more information about *Accepted Manuscripts* in the [Information for Authors](#).

Please note that technical editing may introduce minor changes to the text and/or graphics, which may alter content. The journal's standard [Terms & Conditions](#) and the [Ethical guidelines](#) still apply. In no event shall the Royal Society of Chemistry be held responsible for any errors or omissions in this *Accepted Manuscript* or any consequences arising from the use of any information it contains.



Journal Name

ARTICLE

Effects of Three-Dimensional Mechano-Chemical Tensile Strain on Fast Oxygen Diffusion in Au-Dispersed $\text{Pr}_{1.90}\text{Ni}_{0.71}\text{Cu}_{0.24}\text{Ga}_{0.05}\text{O}_{4+\delta}$

Junji Hyodo^{a,b}*, Ken Tominaga^a, Shintaro Ida^{a,b}, Tatsumi Ishihara^{a,b}*Received 00th January 20xx,
Accepted 00th January 20xx

DOI: 10.1039/x0xx00000x

www.rsc.org/

There has been considerable interest in the effects of strain on electrical conduction in ionic conductors, and it has been suggested that tensile strain in oxide films (2D strain) can significantly increase oxide ion conductivity. Here, we demonstrate the successful generation of 3-dimensional (3D) tensile strain in Pr_2NiO_4 by dispersing Au particles into the grains. The oxide ion diffusivity was increased significantly by the Au dispersion. Redox titration measurements suggest that the 3D tensile strain increased the amount of excess oxygen. Therefore, it is concluded that the mechanical strain changes both oxide ionic carrier concentration and its mobility.

Introduction

Mass transport in nanostructured materials has attracted significant interest because of the potential for improving the performance of solid state electrochemical devices such as solid oxide fuel cells (SOFCs). There are many approaches and ideas for increasing oxide ion conductivity in electrolytes by nanoscale effects, i.e., decreasing the grain size,^[1,2] making thin films of nanoscale thickness,^[3,4] or building a multilayer structure with a hetero junction interface.^[5,8,10–14] The space charge layer (SCL) theory was proposed in order to explain the observed changes in electronic and ionic conductivity.^[6] However, this theory cannot explain the behavior of heavily doped systems based on ZrO_2 and CeO_2 .^[7,8] Another possible reason for nanoscale effects on conductivity is the so-called strain effect.^[9] There have been many reports describing conductivity in epitaxial or highly textured thin oxide ionic conductors with nanoscale thickness.^[10–18] However, for nanofilms, the quality and crystallinity of the film also influence the conductivity, which cannot be described as a simple relationship between tensile strain and ion conductivity.

It is well known that the thermal expansion coefficients of metals and metal oxides are different. Therefore, when a metal and metal oxide are bonded at an elevated temperature and then cooled, a large strain will be introduced at the interface. This introduced strain may be equally induced to the all crystal plane due to the random dispersion state of metal and metal oxide, so a 3-dimensional (3D) tensile strain will be

generated, as shown schematically in Figure 1. The quality of a bulk sintered sample should be independent of the metal dispersion in the grains, so the effects of tensile strain on ion conductivity are more readily observed by dispersing the metal particles into the metal oxide. In order to induce tensile strain, Cu- and Ga-doped $\text{Pr}_2\text{NiO}_{4+\delta}$ (PNCG) and gold particles were chosen, because the thermal expansion coefficients of PNCG ($\alpha = 13.5\text{--}13.8 [10^{-6} \text{K}^{-1}]$) are slightly lower than that of Au ($\alpha = 14.2 [10^{-6} \text{K}^{-1}]$).^[19–21] We have reported the electrical property of Au dispersed PNCG in the previous work, so the detail of ionic transport property is summarized in this report.^[22]

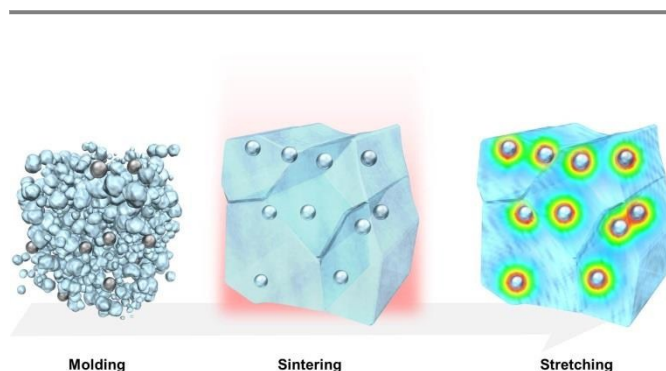


Figure 1. Schematic image of 3-dimensional strain due to metal dispersion in a metal oxide.

Results and Discussions

Wide-angle XRD patterns of x mol% Au-added PNCG pellets are shown in Figure 2a. All samples had the tetragonal structure of the Pr_2NiO_4 -based oxides, regardless of the existence of Au particles. The intensity of the diffraction peaks attributed to Au

^a Department of Applied Chemistry, Faculty of Engineering, Kyushu University, Motoooka 744, Nishi-ku, Fukuoka, 819-0395, Japan

^b International Institute for Carbon-Neutral Energy Research (WPI-I²CNER), Kyushu University, Motoooka 744, Nishi-ku, Fukuoka, 819-0395, Japan

†Electronic Supplementary Information (ESI) available. See

DOI: 10.1039/x0xx00000x

increased with increasing amounts of added Au, suggesting that Au is completely insoluble in the Pr_2NiO_4 base oxides, and

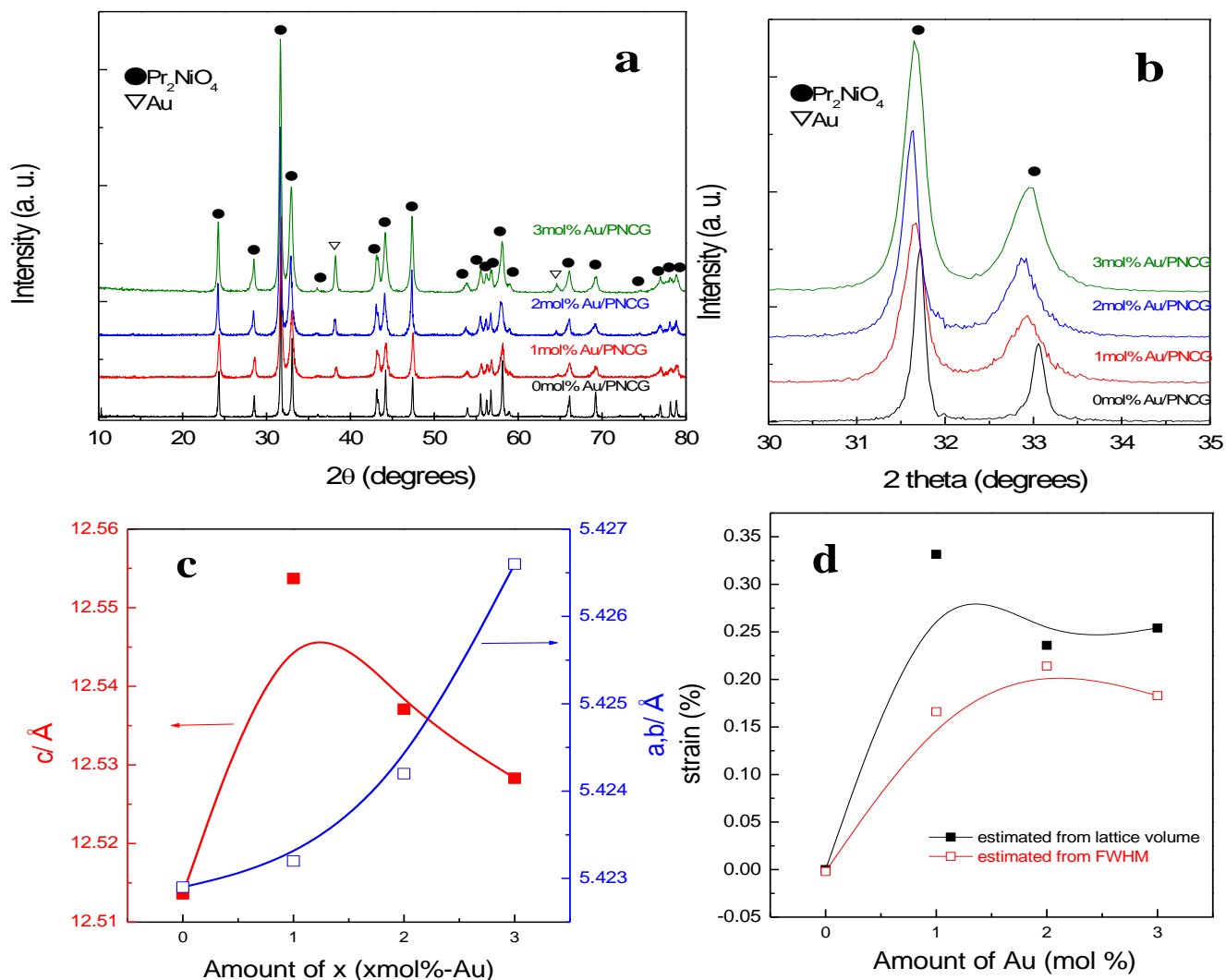


Figure 2. XRD analysis of Au/PNCG. (a) XRD patterns from x mol% Au/PNCG (x=0, 1, 2, 3). (b) Magnified main diffraction peaks of PNCG in the 2-theta region of 30 to 35 degrees. (c) Estimated lattice parameter as a function of the amount of dispersed Au. (d) Strain with different amounts of Au, estimated from the lattice volume (black line) and FWHM (red line) in the Williamson-Hall plot.

that Au was dispersed in the prepared pellets. The residual stress in the PNCG was examined using XRD. Figure 2b shows magnified diffraction peaks in the 2-theta (2θ) range from 30 to 35 degrees. The peak attributed to Pr_2NiO_4 shifted to a lower angle with increasing amounts of dispersed Au until 2 mol%, indicating that the PNCG unit lattice volume was expanded. To discuss the strain in the PNCG, the lattice parameters of the samples were estimated from the diffraction peak positions of the (004) and (220) planes. The dependence of the lattice parameter on the Au content is plotted in Figure 2c. The c-axis elongated with increasing added Au, up to 1 mol%, while the a-axis remained tensile for all Au amounts added. Both peak shift and peak width increased with increasing amounts of added Au, indicating that residual stress remained in the PNCG crystal lattice. To discuss

this strain quantitatively, the strain was also estimated from the full-width at half-maximum (FWHM) of the X-ray diffraction peaks using the Williamson-Hall method.^[23,24] The estimated strain is plotted in Figure 2d. The strain values estimated from the lattice volume are plotted in the same graph for comparison. The obtained values and their trend were similar to those calculated from the lattice constant. The maximum lattice distortion, estimated from the FWHM, was 0.23% at 2 mol% Au. It is well known that the Raman peak shift is sensitive to residual strain. Figure 3b and 3c show a Raman intensity image of 1 mol% Au/PNCG in a selected area at (b) 443 cm^{-1} and (c) 641 cm^{-1} , respectively. Spectra from the (b) and (c) regions are shown in Figure 2d. The spectra varied from grain to grain. One grain has strong peak at 443 cm^{-1} , the other grain has the broad and weak peak at 641 cm^{-1} . According to

the Raman spectrum of bulk PNCG shown in Figure S1, the peak at 641 cm^{-1} seems to be assigned to the PNCG. Moreover, in Figure 3d, the Raman spectrum of Pr_6O_{11} is also shown for reference. The peak in area (b) is close to the peak position Pr_6O_{11} . However, the peak from area (b) was at a slightly higher Raman shift, and no PrO_x peaks were observed in the X-ray diffraction patterns shown in Figure 2a. Therefore, it can be said that this green area was tensile because of the Au dispersion. Spot measurements were also performed at the two points shown in Figure S1, spot (a) was close to aggregated Au, and spot (b) was far from it.

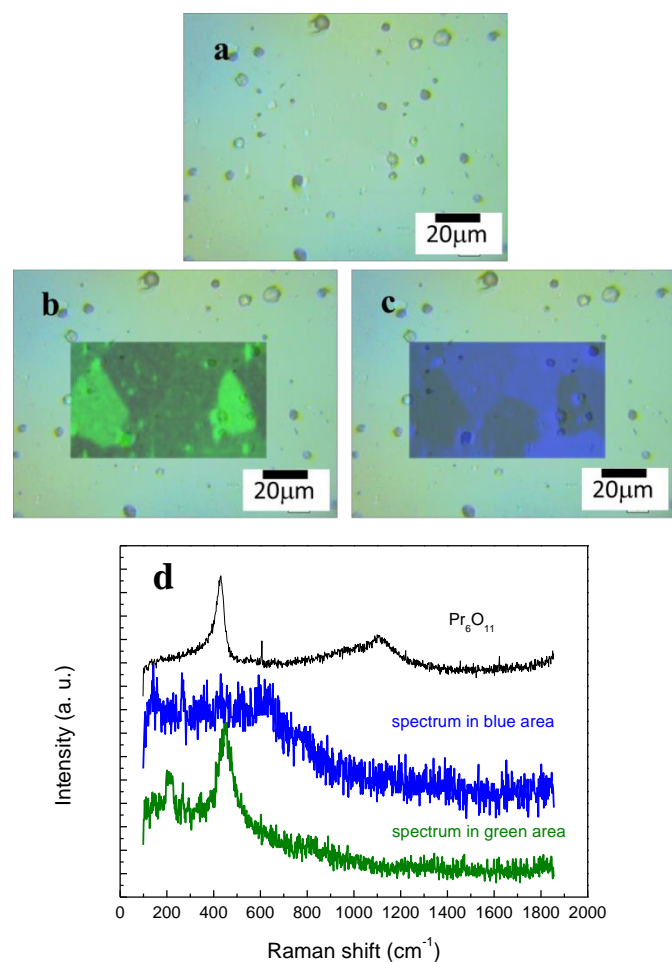


Figure 3. Distribution of Raman peak intensity in 1 mol% Au-dispersed PNCG. (a) A picture of the measured area, (b) the intensity at 443 cm^{-1} , and (c) the intensity at 641 cm^{-1} . (d) Raman spectra from region-(b) (green) and region-(c) (blue). For comparison, the spectrum of Pr_6O_{11} is shown.

For comparison, PNCG without Au dispersion is also shown in Figure S1. The PNCG peaks in the region from 400 to 700 cm^{-1} were broadened, and the regions close to the Au dispersion contained a new peak at 450 cm^{-1} , which is similar peak position to the green area in Figure 2b. Therefore, the high intensity area in Figure 2b suggests a tensile PNCG lattice. This imaging result indicates tensile strain in PNCG was not uniform in PNCG pellets, and that significant strain might be localized

at the interface of Au and PNCG. To check the state of the Au particle dispersion, field emission scanning electron microscopy (FE-SEM) was performed. To clearly observe the

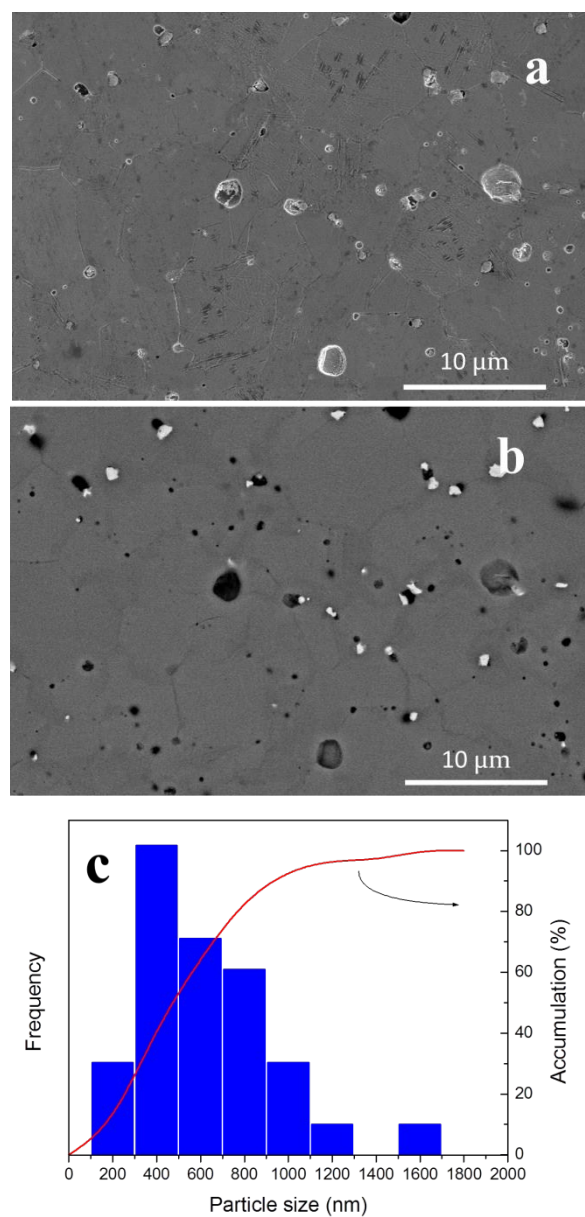


Figure 4. (a) Secondary electron (SE) image of a 1 mol% Au/PNCG surface. (b) Back-scattering electron (BSE) image of a 1 mol% Au/PNCG surface after annealing in air at 1073 K . (c) The distribution of Au particle size in 1 mol% Au/PNCG. (d) 3-dimensional distribution of contrast in an SE image of Au/PNCG. (e) Pore distribution (purple) and Au particle distribution (green) extracted from the contrast. (f) A view

showing a frame format of distribution of Au particles (green) and pores (purple) in bulk PNCG.

grain boundaries, the surface was thermally etched at 1073 K for 2 h in air. Figures 4a and 4b show a secondary electron (SE) image and a backscattered electron (BSE) image, respectively. The SE image shows a dense and smooth sample surface, suitable for the measurement of oxygen transport properties. Because Au is a heavy element, strong contrast was observed

in the BSE image, as shown in Figure 4b. Most of the strong contrast points were observed at the PNCG grain boundary. The observed Au particle sizes were distributed over a wide range from 0.2-1.5 μm , as shown in Figure 4c. The crystallite sizes of the Au, as estimated using Scherer's equation to analyze the XRD results, were 36.9-40.8 nm, indicating that the Au particles were aggregated and non-uniform in size. Figures 4d-4f show 3-dimensional SEM images of 1 mol% Au/PNCG.

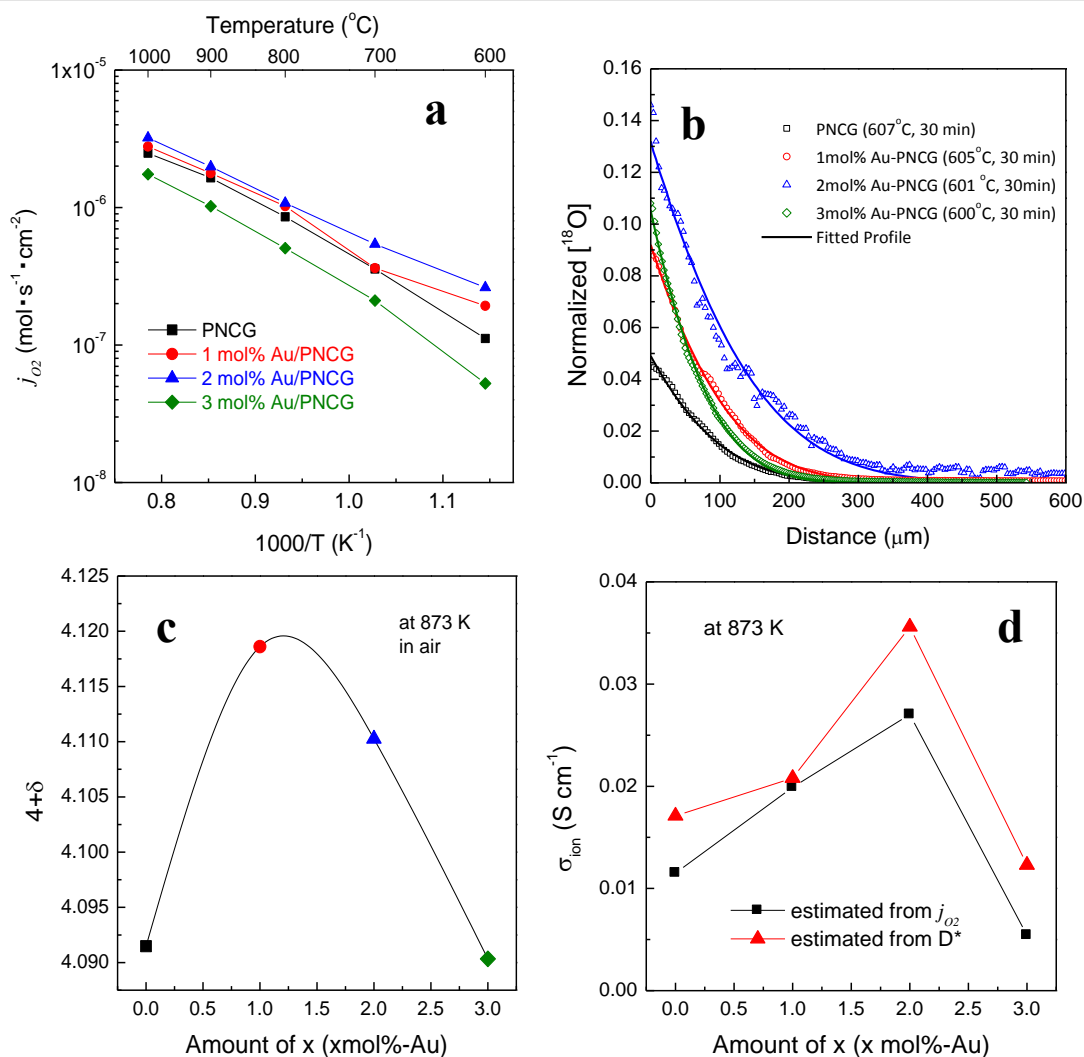


Figure 5. (a) Arrhenius plot of oxygen flux (j_{O_2}) with different Au amounts. (b) Depth profile of ^{18}O fraction with different amounts of Au dispersion. (c) Oxygen nonstoichiometric composition in Au/PNCG at 873 K with respect to the amount of dispersed Au. (d) Oxide ion conductivity estimated from oxygen permeability (j_{O_2}) and oxygen tracer diffusivity (D^*).

Because of the available contrast in the SEM images, Au particles and pores can be easily distinguished. The sample was highly dense, and the volume of observed pores was only 0.2 vol% of the measured space. The volume of Au particles was 0.6 vol%, which agreed well with the expected value based on the composition (0.5 vol%). Furthermore, the large spaces without any Au particles and the regions in which Au was concentrated could both be observed. The presence of large spaces devoid of Au particles demonstrates a poor

uniformity of Au dispersion in the Au/PNCG pellets. This dispersion state and the aggregation of Au particles are both explained by the fact that the melting temperature of Au is lower than the sintering temperature of the Au/PNCG pellets. Changes in particle size could be the origin of the non-uniform strain distribution in the Raman mapping shown in Figure 3.

In order to confirm the effects of strain on oxygen diffusivity, oxygen permeation measurements were performed under the bulk diffusion limited condition.^[20] Figure 5a shows an

Arrhenius plot of the oxygen flux with different amounts of Au. Obviously, enhanced oxygen transport with increasing amounts of added Au was confirmed. The difference between samples with and without Au addition became more significant with decreasing temperature.

The apparent activation energies for oxygen permeation are listed in Table 1. Evidently, the activation energy was reduced by the addition of Au until the amount of Au reached 3 mol%. A doubled oxygen permeation flux was achieved by dispersing 2 mol% Au in PNCG at 873 K, indicating that the tensile strain in the PNCG lattice increased oxygen permeation. Since oxygen permeation is controlled by the concentration and mobility of interstitial oxygen, further study of the detailed effects of tensile strain on oxygen diffusivity was performed using ^{18}O tracer diffusion. The depth profiles for x mol% Au/PNCG ($x=0, 1, 2, \text{ and } 3$) are shown in Figure 5b, and the estimated oxygen tracer diffusivity (D^*) and the surface exchange coefficient (k^*) are summarized in Table 1. The D^* values were clearly increased by dispersing Au, and their enhancement relative to that of PNCG without Au was similar to that of the oxygen permeation rate. Additionally, a nonstoichiometric oxygen composition in PNCG at 873 K was measured using redox titration to reveal the oxide ion concentration. Figure 5c shows the Au content dependence of oxygen composition in x mol% Au/PNCG.

Table 1. Estimated values of the apparent activation energy based on the oxygen permeation rate, and D^* and k^* values at 873 K estimated from Figure 5(b).

Amount of Au [mol%]	Activation energy estimated from O_2 permeation rate [eV]	D^* at 873 K [$10^{-8} \text{ cm}^2 \text{ s}^{-1}$]	k^* at 873 K [$10^{-7} \text{ cm s}^{-1}$]
0	0.72	4.28	2.21
1	0.64	5.18	4.72
2	0.58	8.87	9.15
3	0.80	3.07	4.19

Increased interstitial oxygen was also confirmed in Au-dispersed PNCG, and its dependence on Au content was similar to that of the c -axis of the PNCG structure. One reason for the improved oxygen permeability shown in Figure 5a was increased oxygen hyperstoichiometry, and δ value at 873 K was achieved the maximum at 1 mol% Au. Furthermore, oxide ion mobility improved as well, and its maximum value was obtained at 2 mol% Au/PNCG. This result suggests that the tensile strain increased not only the interstitial oxygen concentration but also the oxygen mobility. Decreased ion mobility in 3 mol% Au/PNCG may be the reason for the blocked ion migration by the metallic Au, because the Au is not oxidized, and it is difficult for oxygen to diffuse through metallic gold. To check the reliability of the obtained oxygen tracer diffusivity and hyper stoichiometry in PNCG, oxide ion conductivity at 873 K was estimated from the permeation rate using Wagner equation, and tracer diffusivity and oxygen content using the Nernst-Einstein relation, respectively.^[25,26] The obtained values agree well, as shown in Figure 5d, suggesting reliable oxide ion transport. As mentioned earlier,

the tensile strain in PNCG is significant at lower temperatures because the lattice probably relaxes at the sintering temperature. Therefore, decreasing the temperature induced tensile strain in the PNCG, potentially enhancing both oxygen concentration and mobility.

On the other hand, enhancements of the k^* values in the oxygen exchange kinetics were also observed. The maximum value was again achieved in PNCG with 2 mol% Au addition, and this value was about 4 times that of PNCG bulk. Because Au is generally inactive with respect to the oxygen exchange reaction, this enhancement of the k^* value can be assigned to strain effects in the PNCG. This suggests that the tensile strain improved not only mass transport, but also oxygen exchange at the surface. The relationship between surface exchange coefficients and the state of surface with strain condition is now under investigation, and will be reported in the future.

Conclusions

In this study, the oxide ionic conductivity measurement in Au dispersed PNCG was performed. It is found that tensile strain in PNCG affects the both carrier concentration and mobility. Although the Au dispersion was not uniform, the positive effects of tensile strain on oxide ion mobility were observed. Furthermore, the tensile strain also affected the surface exchange property. If a better dispersion of fine Au particles could be achieved, it could enable to create the higher oxide ionic conductor with 3-dimensionally uniform strain.

Experimental

Pellets of x mol% Au-added $\text{Pr}_{1.90}\text{Ni}_{0.71}\text{Cu}_{0.24}\text{Ga}_{0.05}\text{O}_{4+\delta}$ (x mol% Au/PNCG, $x = 0, 1, 2, 3$) were prepared by solid-state reaction using $\text{Pr}(\text{NO}_3)_3 \cdot 6\text{H}_2\text{O}$ (99.9 %, Mitsuwa Chemicals Co., Ltd., Japan), $\text{Ni}(\text{CH}_3\text{COO})_2 \cdot 4\text{H}_2\text{O}$ (98 %, Wako Pure Chemical Industries, Ltd., Japan), $\text{Cu}(\text{NO}_3)_2 \cdot 3\text{H}_2\text{O}$ (99 %, Wako Pure Chemical Industries, Ltd., Japan), $\text{Ga}(\text{NO}_3)_3 \cdot n\text{H}_2\text{O}$ (99.99 %, Mitsuwa Chemicals Co., Ltd., Japan), and $\text{HAuCl}_4 \cdot 4\text{H}_2\text{O}$ (99.0 %, Kishida Chemical Co., Ltd., Japan) as starting materials with stoichiometric amount. The n value in $\text{Ga}(\text{NO}_3)_3 \cdot n\text{H}_2\text{O}$ was determined using thermogravimetric analysis. The resulting mixtures were dissolved in deionized water, and dried with mixing. The resulting powders were heated at 673 K to remove NO_x . The obtained powders were then calcined at 1073 K for 6 hours, and pressed into 20-mm-diameter disks. The prepared disks were sintered at 1523 K for 6 hours, and were sufficiently dense as obtained, with relative densities above 90%. The crystal structures of the prepared disks were measured by X-ray diffraction (RINT2500, Rigaku Co.) with $\text{Cu-K}\alpha$ radiation after polishing their surfaces. Laser Raman spectrometry was also performed on surface-polished 1 mol% Au/PNCG with RENISHAW equipment (model: in Via Raman Microscope). Rapid imaging measurements were performed with a line-shape laser (so-called Streamline mode) which can achieve the fast Raman mapping of large areas. For the oxygen permeation measurements, the prepared pellets were polished to 0.5 mm

thick. The measurement details were reported elsewhere.^[20] It is noted that the electronic conductivity of PNCG is sufficiently high for oxygen permeation, and that oxygen permeation rate is limited by bulk oxygen diffusivity.^[20] The oxygen tracer diffusivity and surface exchange coefficient were estimated using isotope exchange and depth profiling. The isotope oxygen was exchanged at 873 K for 30 min. The exchange oxygen partial pressure was 13.3 kPa, and the temperature was monitored with a K-type thermocouple located close to the sample. The oxygen isotope diffusion profile was obtained by secondary ion mass spectrometry (SIMS) using an ATOMIKA 4100 quadrupole-base analyzer in linescan mode with a cesium ion primary source (Cs⁺) at 5 keV. The oxygen tracer diffusion coefficient and the oxygen surface exchange coefficient were estimated by fitting to a diffusion equation based on Fick's second law.^[27] The nonstoichiometric oxygen compositions in x mol% Au/PNCG (x = 0, 1, 2, 3) were measured by redox titration. The samples were annealed in air at 873 K for more than 10 h, and then quenched. The obtained samples were dissolved in HCl with excess KI, and the precipitated I₂ was titrated using Na₂S₂O₃ solution.

Acknowledgements

This work was supported in part by Grant-in-Aid for Scientific Research (S) No. 24226016 and the Advanced Low Carbon Technology Research and Development Program (ALCA).

Notes and references

- P. Mondal, A. Klein, W. Jagermann, H. Haln, *Solid State Ionics*, 1999, **118**, 331-339.
- G. Knoner, K. Reimann, R. Röwer, U. Södervall, H.-E. Schaefer, *Proc. Natl. Acad. Sci. USA*, 2003, **100** (7), 3870-3873.
- I. Kosacki, C. M. Roulea, P. F. Becher, J. Bentley, D. H. Lowndes, *Solid State Ionics*, 2005, **176**, 1319-1326.
- X. Guo, E. Vasco, S. Mi, K. Szot, E. Wachsman, R. Waster, *Acta Materialia*, 2005, **53**, 5161-5166.
- N. Sata, K. Eberman, K. Eberl, J. Maier, *Nature*, 2000, **408**, 946.
- J. Maier, *Nat. Mater.*, 2005, **4**, 805-815.
- A. Tschope, S. Kilassonia, R. Birringer, *Solid State Ionics*, 2004, **173**, 57-61.
- S. Azad, O. A. Marina, C. M. Wang, L. Saraf, *Appl. Phys. Lett.*, 2005, **86**, 131906.
- J. A. Kilner, *Nat. Mater.*, 2008, **7**, 838-839.
- A. Peters, C. Korte, D. Hesse, N. Zakhovov, *Solid State Ionics*, 2007, **178**, 67-76.
- C. Korte, A. Peters, J. Janek, D. Hesse, N. Zakhovov, *Phys. Chem. Chem. Phys.*, 2008, **10**, 4623-4635.
- J. Garcia-Barriocanal, A. Rivera-Calzada, M. Varela, Z. Sefrioui, E. Iborra, C. Leon, S. J. Pennycook, J. Santamaria, *Science*, 2008, **321**, 676-680.
- A. Cavallaro, M. Burriel, J. Roqueta, A. Apostolidis, A. Bernardi, A. Tarancon, R. Srinivasan, S. N. Cook, H. L. Fraser, J. A. Klnr, D. W. McComb, J. Santiso, *Solid State Ionics*, 2010, **181**, 592-601.
- D. Pergolesi, E. Fabbri, S. N. Cook, V. Roddatis, E. Traversa, J. A. Kilner, *ACS NANO*, 2012, **6** (12), 10524-10534.
- A. Kushima, B. Yildiz, *J. Mater. Chem.*, 2010, **20**, 4809-4819.
- M. Burriel, J. Santiso, M. D. Rossell, G. van Tendeloo, A. Figueras, G. Garcia, *J. Phys. Chem. C*, 2008, **112**, 10982-10987.
- M. Burriel, G. Garcia, J. Santiso, J. A. Kilner, R. J. Chater, S. J. Skinner, *J. Mater. Chem.*, 2008, **18**, 416-422.
- H. Matsumoto, Y. Furuya, S. Okada, T. Tanji, T. Ishihara, *Electrochem. Solid-State Lett.*, 2007, **10**, 11-13.
- T. Ishihara, K. Nakashima, S. Okada, M. Enoki, H. Matsumoto, *Solid State Ionics*, 2008, **179**, 1367-1371.
- T. Ishihara, N. Sirikanda, K. Nakashima, S. Miyoshi, H. Matsumoto, *J. Electrochem Soc.*, 2010, **157** (1), B141-B146.
- M. Yashima, M. Enoki, T. Wakita, R. Ali, Y. Matsushita, F. Izumi, T. Ishihara, *J. Am. Chem. Soc.*, 2008, **130**, 2762-2763.
- J. Hyodo, K. Tominaga, J.-E. Hong, S. Ida, T. Ishihara, *J. Phys. Chem. C*, 2015, **119**, 5-13.
- G. K. Williamson, W. H. Hall, *Acta Metal*, 1953, **1** (1), 22-31.
- J. L. M. Rupp, C. Solenthaler, P. Gasser, U. P. Muecke, L. J. Gauckler, *Acta Materialia*, 2007, **55**, 3505-3512.
- F. Mauvy, J. M. Bassat, E. Boehm, P. Dordor, J. P. Loup, *Solid State Ionics*, 2003, **158**, 395-407.
- J. A. Lane, S. J. Benson, D. Waller, J. A. Kilner, *Solid State Ionics*, 1999, **121**, 201-208.
- J. Crank, *The Mathematics of Diffusion*, 2nd ed., Oxford University Press, 1975.

